

Morphological Studies of the Murine Heart Based on Probabilistic and Statistical Atlases

D. Perperidis¹, E. Bucholz², G. A. Johnson², and C. Constantinides¹

¹Mechanical and Manufacturing Engineering, University of Cyprus, Nicosia, Aglantzia, Cyprus, ²Radiology, Center for In Vivo Microscopy, Duke University Medical Center, Durham, North Carolina, United States

Introduction

MRI has significant potential for evaluating and quantifying cardiac function and dysfunction in the mouse. Recent advances in high-resolution cardiac MR imaging techniques for the study of normal and transgenic mice [1-3] have led to the development of human [4,5] and mouse [6] atlas-based approaches to describe anatomic structures and their function. Despite such prior efforts, only limited attempts exist for construction of accurate, high spatial and temporal resolution computerized atlases that capture the functional and morphological variability of mouse hearts across different strains, types, under controlled physiological conditions, and under inhalational anesthesia, a prerequisite for non-invasive imaging studies, including MRI. This study compares interstrain morphological features of the mouse heart (left and right ventricular [LV,RV] muscle and blood cavities), based on constructed morphometric maps and atlases using Principal Component Analysis (PCA) of the CB57L/6 and DBA mouse strains.

Methods

Physiology: Ten C57BL/6J and five DBA mice were anesthetized using isoflurane (ISO) and allowed to breathe freely throughout the study. ECG and breathing rate were monitored using an SA Instruments Inc. system (Edison, NJ, USA). Heart rate was maintained between 450-550 beats per minute by adjusting the mixture of ISO and oxygen. A rectal probe monitored and maintained stable core body temperature in the magnet ($37 \pm 0.5^\circ\text{C}$).

Imaging: Work was performed at 7T with a GE EXCITE console (EPIC 12.4). A custom-made $2.5 \times 3 \text{cm}^2$ transmit/receive coil maximized SNR. A 4D radial MRI pulse sequence was implemented and optimized to reduce TE and TR to $300 \mu\text{s}$ and 2.4ms respectively, as published in [2]. Eight phases of the heart cycle were acquired at temporal resolution of 9.6ms and at spatial resolution of $87\text{-}110 \mu\text{m}^3$ in 31 minutes, with $\text{BW} = \pm 125 \text{kHz}$, and flip angle $= 45^\circ$. A non-uniform fast Fourier transformation performed regridding reconstruction using a least squares optimized kernel for interpolation. Raw data were reconstructed offline.

Image Processing: Probabilistic and statistical atlases were constructed by: (a) seed-point spline contour segmentation of the left/right ventricular muscle and cavities (Analyze 7.0, USA) from end-diastolic short axis cardiac MRI. Binary masks were generated, intensity normalized, and converted to the .gipl format using ImageJ (ImageJ,NIH,USA). Uncertainties in the apical regions were corrected with the RVIEW program (IXICO, UK) and 3D volume stacks constructed; (b) alignment of all mouse models to a common coordinate system using a 5-landmark affine registration (ITK software for IXICO), and matching of extracted landmarks using non-linear splines; (c) filtering with a 2D- Gaussian filter with $\sigma=2$. The probabilistic atlas was formed by averaging the transformed images and the statistical atlas by approximating the distribution of landmarks with a linear model $q = \bar{q} + \Phi b$ where \bar{q} is the average landmark vector, b is the shape parameter vector and Φ is the eigenvector matrix, computed by PCA.

Results and Discussion

Figure 1 shows typical results from the seed-point segmentation and five-point landmark registration. Figure 2 (top) shows the probabilistic atlas of the CB57 mice. The atlas confirms mean probability of pixel location belonging to myocardium for septal ($\text{Pr}=0.47/0.47/0.29$), inferior ($\text{Pr}=0.38/0.38/0.24$), lateral ($\text{Pr}=0.52/0.48/0.25$), anterior ($\text{Pr}=0.34/0.33/0.28$) for basal/mid-ventricular/apical slices. Areas with maximum probabilities are near the septal and lateral myocardial borders. Additionally, a gradient probability variation exists from base-apex with apical locations exhibiting significantly lower mean probabilities compared to basal locations. Similar patterns were observed in DBA mice. Figure 2 (Bot) shows the most significant modes of variation of the left ventricle for (left) CB57 and (right) DBA mice. For myocardium in CB57 mice, the three most significant modes reflect variability in size (34%), in apical direction (25%), and basal LV blood pool size combined with LV direction (15%). For DBA mice, 42% explains shape variation, 22% right ventricular position, and 19% apical position. Inter-strain comparison of RV yielded variability differences that can be accounted for the size and position of the right ventricle, especially at apical locations. Apart from possible existence of intrinsic physiological variability due to cardio-depressive anesthesia effects, results reason in favor of variability in the apical location in both strains. Regarding the statistical atlases, no major inter-strain differences were observed.

References: 1) Ruff, J. et al. MRM 40:43-8, 1998. 2) Bucholz, E. et al. MRM 60:111-8, 2008. 3) Chien, KR. et al. Circ. Res. 88:546-9,2000. 4) Perperides, D. et al. Med. Imag. An. 9(5):441-456, 2005. 5) Cootes, TF. et al. 61(1):38-59, 1995. 6) Ali, A. et al. Neuroimage 27:425-435, 2005.

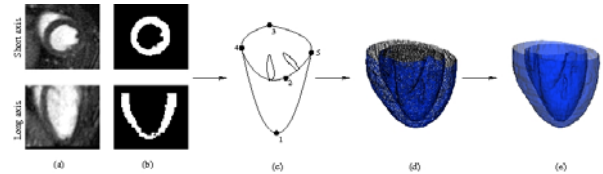


Figure 1: (a) Typical mid-ventricular short and long-axis images from a mouse heart; (b) segmentation and corresponding binary masks; (c) five-point landmark-marked mesh used for global registration; (d) construction of the 3D mesh volumetric dataset, and (e) 3D model surface rendition.

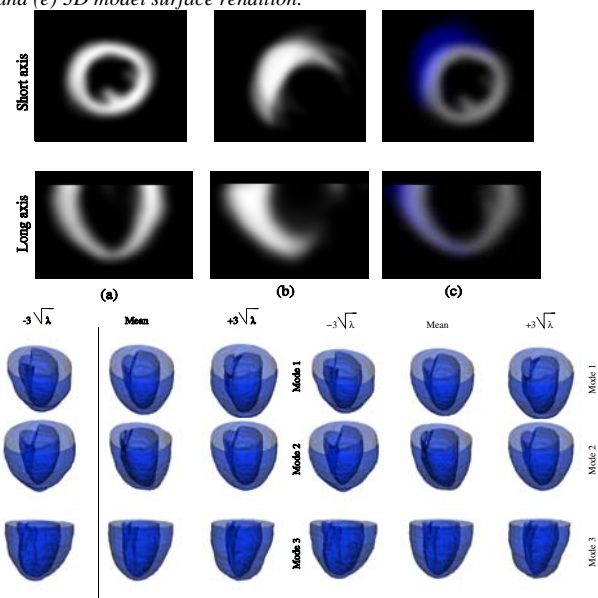


Figure 2: (Top) Probabilistic atlases for CB57L mice: (a) Short and long axis views of the LV; (b) corresponding views of the RV; (c) probabilistic atlases depicted in (a, b) fused in a single dataset. (Bottom) 3D model renditions depicting the three most significant modes of shape deviation of the LV statistical atlas for (Left) CB57L/6J and (Right) DBA mice.

Supported in part by NCRR/NCI P41 RR005959, U24 CA092656 and by grant 'HEART', from the Hellenic Bank.